MODELING AND SIMULATION OF NANOFLUID TRANSPORT VIA BIO-ELASTIC SHEETS

M.J. Uddin [a], *, A. Sohail [b], O. Anwar Bég [c] , A.I.Md. Ismail [d]

a American International University–Bangladesh, Banani, Dhaka 1213, Bangladesh
b Department of Mathematics, COMSATS Institute of Information Technology, Lahore, Pakistan
c Fluid Mechanics and Propulsion, Aeronautical and Mechanical Engineering, Room G77, Newton Building, School of Computing, Science and Engineering (CSE), University of Salford, M54WT, UK
d School of Mathematical Sciences, Universiti Sains Malaysia, 11800 Penang, Malaysia

ABSTRACT: *The field of bio-nanofluidics research has spanned over the past decade with a variety of promising applications. We investigate the ``laminar boundary layer flow'' of a Newtonian nanofluid past a moving extendable/contractable horizontal plate with surface velocity and thermal slip effects. The passively controlled nanofluid model (PCM) is considered. Such models are physically more realistic as compared to the "actively controlled models" (ACM). Using Lie symmetry group method, the governing equations are reduced by a set of highly coupled nonlinear ODE's with thermo-solutal coupled boundary conditions. The reduced equations are solved numerically by a generalized collocation method. The influences of the emerging parameters on the local skin friction factor and the local Nusselt number are depicted numerically. The skin friction is decreased as the thermo-phoresis and buoyancy ratio parameters are decreased. The heat transfer rates reduce with thermophoresis and buoyancy ratio parameters. Velocity slip also leads to a rise in wall temperature gradient. This study is relevant to near-wall flows in nanofluid fuel cells, nano-materials processing etc.*

1. INTRODUCTION

There has been immense progress in the improvement of energy-proficient heat transfer fluids over the last two decades. In this quest, *nanofluids* have attracted significant attention due to their ability to enhance thermal conductivity very substantially in many different scenarios. **Choi (1995)** discussed heat transfer nanofluids with more efficient thermal conductivity results as compared to the conventional heat transfer fluids. Nanofluids are a homogenous mixture of base fluid and nanoparticles. On the other hand some commonly used nanoparticles are particles of metals, nitrides and carbides etc. An inspection of the current scientific literature, nanofluids can be used in aircraft, automobiles, fuel cells and many engineering systems. Due to nanometer sized materials nanofluids have unique physical and chemical properties. Nanofluids are implemented in many industries e.g. in petroleum reservoir flooding (e.g. **Suleimenov et al. (2014)** who showed a reduction of surface tension on an oil boundary is attained with nanofluids), cooling of nuclear reactors, melt-spinning and manufacture of plastic and rubber sheets. They are further known to be employed in the extrusion of a polymer sheet from a die and crystal growth, refrigeration (e.g. **Coumaressin and Palaniradja (2014)**, wherein evaporator heat transfer coefficient is shown to increase with the use of nanoparticles e.g. copper oxide), hybrid fuel cells, sterilization of materials (e.g. silver oxide nanofluids), enhanced cooling of metallic plates in a cooling bath, treatment of paper drying systems and in combustion fuel technologies (e.g. **Sonewane et al. (2012)** who consider doping of jet fuels). The important features of the nanofluids include higher thermal conductivity as compared to the base fluid and stable nature of the suspension. The volume fraction of nanoparticles is usually engineered to be 3% to 5% (**Das et al. 2007**), so that the nanofluid exhibits mechanical behavior similar to the base fluid. Different models have been proposed to address the large increase in thermal conductivity. The factors responsible for the increase in thermal conductivity in nanofluids include (a) dispersion of nanoparticles (**Buongiorno 2006**) (b) the turbulence due to the presence of nanoparticles (**Pak and Cho 1988**) and (c) the effect of the rotation of the nanoparticles (**Xuan and Li 2003**). A comprehensive theory is required for the estimation of the thermal conductivity of a nanofluid. Theoretical models such as (**Maxwell-Garnett 1904**, **Wang et al. 2003**) give much lower values than those acquired at the laboratory level. It is now established (from experiments and theoretical results) that for forced convective nanofluid flow heat transfer characteristics enhances, whereas reverse observation is noticed in the case of natural convection. Convective heat and mass transfer of nanofluid flow have received attention of researchers owing to it wide range of applications such as bio-convection in microbial fuel cells, the delivery of nano-drug, electronics cooling, solar energy etc. Two

available models which are easily incorporated into the framework of boundary layer flows of nanofluids are (i) the **Buongiorno (2006)** model in which Brownian motion and thermophoresis effects are included and (ii) the **Tiwari and Das (2007)** model which can be utilized to study the behavior of nanofluids considering the solid volume fraction. Many investigators deployed these two models to study various flow phenomena external to various geometries subject to various boundary conditions. As an example, **Kuznetsov and Nield (2010)** obtained similarity solution for natural convection flow of a nanofluid along a vertical plate. **Nield and Kuznetsov (2009)** further studied the Cheng–Minkowycz problem of natural convection past a vertical plate in a porous medium for nanofluids. **Nield and Kuznetsov (2011)** further extended the same problem for binary nanofluids, including the effects of cross diffusion. Very recently, **Kuznetsov and Nield (2014)** revised their earlier model by incorporating a *passively controlled* boundary condition. Reviews have been conducted of the latest developments in nanofluid technology and are available in the papers of **Wang and Mujumdar (2007), Das and Choi (2009), Kakac and Pramuanjaroenkij (2009)**, **Adnan *et al.* (2014), Mahdi *et al.* (2015), Mauro *et al.* (2015), Ali *et al.* 2015, Sheikholeslami *et al.* (2015)** etc. and in the monographs of **Tiwari and Das (2007), Sattler (2010), Murshed *et al.* (2011) and Minkowycz *et al.* (2012)**. These efforts identify, not least, numerous further problems which require mathematical (and experimental) simulation whether in terms of nanofluid type, geometry, boundary condition or indeed combinations of these aspects.

The vast majority of investigations have generally focused analysis on natural convective flow of nanofluids from vertical surfaces. However, the natural convective flow of nanofluids from a *horizontal surface* is also of great interest in engineering devices and processes. To achieve more physically realistic and practically applicable results, in the present article we address the composite effects of velocity slip, thermal slip and zero mass flux boundary conditions on the boundary layer flow of nanofluid over an upward facing horizontal sheet (plate). In addition to the imposition of modified slip and solutal boundary conditions, sheet stretching/shrinking is also an important characteristic in manufacture of nanomaterials (**Ferdows *et al.* 2014**), and indeed in compliant surfaces in next-generation "green" fuel cells (**Tominaka *et al.* 2009**). An experimental investigation in materials extrusion carried by **Vleggaar (1977)** revealed that the surrounding fluid motion can be idealized by a tangentially moving boundary with a velocity proportional to linear/nonlinear function of the distance from the slit. Hence to improve the accuracy of wall conditions, we have incorporated the simultaneous effects of velocity slip, Newtonian heating and zero mass flux boundary conditions on the boundary layer flow of

nanofluid over an upward facing nonlinearly radiating horizontal stretching sheet. Lie group analysis is used to determine the *similarity form* of the governing boundary layer equations. Key parameters which influence the heat, mass and momentum transfer processes are shown to be *buoyancy ratio parameter* (which is a measure of the ratio of the buoyancy force arising due to the density difference between the nanoparticle and the base fluid and the buoyancy force due to the thermal expansion of the base fluid), the *Brownian motion parameter* (which gives information about the energy transport by Brownian diffusion) and the *thermophoretic parameter* (that gives a measure of the energy transport due to thermophoresis) and their effect on the fluid velocity and heat transfer rate are discussed. Furthermore the effect of the Lewis number and of course multiple slip conditions on flow characteristics is also elucidated in detail. Verification of the present collocation numerical solutions is achieved where possible with earlier published results.

2. METHODOLOGY

2.1 Materials

A moving horizontal stretching/shrinking sheet in the quiescent free stream is considered. A Cartesian coordinate system ($\bar{x}, \bar{y}$) is used in which the $\bar{x} -$ axis is measured along the plate and the $\bar{y} -$ axis is directed normal to the plate. It is assumed that sheet velocity is

$$\bar{u}_w\left(\bar{x}/L\right) = \lambda U_r \left(\frac{\bar{x}}{L}\right)^{1/5}, \quad \lambda > 0$$ for stretching sheet whilst $\lambda < 0$ shrinking sheet, L is the

characteristics length of the sheet, U_r is an arbitrary reference velocity. The flow model and coordinates system is shown in **Fig.1**. The temperature T_w is assumed at the surface, whereas, T_∞, C_∞ and n_∞ are assumed as their ambient values. Neglecting viscous dissipation in the energy equation, we consider passively controlled (PC) boundary conditions proposed by **Kuznetsov and Nield (2014)**. In addition we have also considered the case when the sheet is subjected to actively controlled boundary conditions (AC) (to compare our results with the literature). The variables are $\overset{1}{V}$: the velocity vector, T: the temperature, C: the nanoparticle volume fraction

$$\nabla \cdot \overset{1}{V} = 0, \tag{1}$$

$$\rho\left[\frac{\partial \overset{1}{V}}{\partial t} + \left(\overset{r}{V} \cdot \nabla\right)\overset{r}{V}\right] = -\nabla p + \nu \nabla^2 \overset{r}{V} + \left[C\rho_p + (1-C)\left\{\rho_f\left(1 - \beta(T - T_\infty)\right)\right\}\right]\overset{r}{g}, \tag{2}$$

$$\left(\rho\, c_{\bar{p}}\right)_f \left(\frac{\partial T}{\partial t}+\overset{\mathbf{r}}{V}\cdot\nabla T\right)=k\nabla^2 T+\left(\rho c_p\right)_p\left[D_B\,\nabla C\cdot\nabla T+\left(\frac{D_T}{T_\infty}\right)\nabla T\cdot\nabla T\right], \tag{3}$$

$$\frac{\partial C}{\partial t}+\bar{V}\cdot\nabla C=D_B\,\nabla^2 C+\left(\frac{D_T}{T_\infty}\right)\nabla^2 T. \tag{4}$$

$$\rho\left[\frac{\partial\overset{\mathbf{l}}{V}}{\partial t}+\left(\overset{\mathbf{r}}{V}\cdot\nabla\right)\overset{\mathbf{r}}{V}\right]=-\nabla\,\bar{p}+\nu\nabla^2\overset{\mathbf{r}}{V}+\left[\left(C-C_\infty\right)\left(\rho_{\bar{p}}-\rho_f\right)+\left(1-C_\infty\right)\rho_f\,\beta\left(T-T_\infty\right)\right]\overset{\mathbf{r}}{g} \tag{5}$$

The boundary layer approximation yields:

$$\frac{\partial\bar{u}}{\partial\bar{x}}+\frac{\partial\bar{v}}{\partial\bar{y}}=0, \tag{6}$$

$$\rho_f\left(\bar{u}\,\frac{\partial\bar{u}}{\partial\bar{x}}+\bar{v}\,\frac{\partial\bar{u}}{\partial\bar{y}}\right)=-\frac{\partial\bar{p}}{\partial\bar{x}}+\mu\frac{\partial^2\bar{u}}{\partial\bar{y}^2}, \tag{7}$$

$$-\frac{\partial\bar{p}}{\partial\bar{y}}+\left[\left(1-C_\infty\right)\rho_f\,g\,\beta\left(T-T_\infty\right)-\left(\rho_{\bar{p}}-\rho_f\right)g\left(C-C_\infty\right)\right]=0, \tag{8}$$

$$\bar{u}\frac{\partial T}{\partial\bar{x}}+\bar{v}\frac{\partial T}{\partial\bar{y}}=\alpha\frac{\partial^2 T}{\partial\bar{y}^2}+\tau\left[D_B\,\frac{\partial C}{\partial\bar{y}}\frac{\partial T}{\partial\bar{y}}+\left(\frac{D_T}{T_\infty}\right)\left(\frac{\partial T}{\partial\bar{y}}\right)^2\right], \tag{9}$$

$$\bar{u}\frac{\partial C}{\partial\bar{x}}+\bar{v}\frac{\partial C}{\partial\bar{y}}=D_B\,\frac{\partial^2 C}{\partial\bar{y}^2}+\left(\frac{D_T}{T_\infty}\right)\frac{\partial^2 T}{\partial\bar{y}^2}, \tag{10}$$

where $\alpha=\dfrac{k}{\left(\rho\,c_{\bar{p}}\right)_f}$ is the thermal diffusivity of the fluid and $\tau=\dfrac{\left(\rho\,c_{\bar{p}}\right)_{\bar{p}}}{\left(\rho\,c_{\bar{p}}\right)_f}$ is a parameter.

The appropriate boundary conditions are, following **Kuznetsov and Nield (2014)**:

$$\bar{u}=\lambda\,\bar{u}_w\left(\bar{x}/L\right)+\bar{u}_{\text{slip}},\ \bar{v}=0,\ T=T_w\left(\bar{x}/L\right)+T_{\text{slip}}\left(\bar{x}/L\right),\ D_B\frac{\partial C}{\partial\bar{y}}+\frac{D_T}{T_\infty}\frac{\partial T}{\partial\bar{y}}=0\ \text{at}\ \bar{y}=0,$$
$$\bar{u}\to 0,\ T\to T_\infty,\ C\to C_\infty,\ \bar{p}\to\bar{p}_\infty\ \text{as}\ \bar{y}\to\infty. \tag{11}$$

Here $(\bar{u},\bar{v})$: the velocity components along the $\bar{x}$ and $\bar{y}$ - axes, $\bar{u}_w\left(\bar{x}/L\right)=\lambda U_r\left(\dfrac{\bar{x}}{L}\right)^{1/5}$: velocity

of the plate, L: characteristic length of the plate, $U_r=\dfrac{\alpha}{L}Ra^{2/5}$:the characteristic velocity,

$\bar{u}_{\text{slip}} = \dfrac{\mu}{\rho} N_1 (\bar{x}/L) \dfrac{\partial \bar{u}}{\partial \bar{y}}$: linear slip velocity, $N_1 \left(\dfrac{\bar{x}}{L} \right) = \left(N_1 \right)_0 \left(\dfrac{\bar{x}}{L} \right)^{2/5}$: velocity slip factor with $\left(N_1 \right)_0$

constant velocity slip factor, $T_{\text{slip}} \left(\dfrac{\bar{x}}{L} \right) = D_1 \left(\dfrac{\bar{x}}{L} \right) \dfrac{\partial T}{\partial \bar{y}}$: thermal slip, $D_1 \left(\dfrac{\bar{x}}{L} \right) = \left(D_1 \right)_0 \left(\dfrac{\bar{x}}{L} \right)^{2/5}$: thermal

slip factor, $\left(D_1 \right)_0$ constant thermal slip factor, $\lambda > 0$ corresponds to a stretching (extending) sheet, $\lambda < 0$ represents a shrinking (contracting) sheet and $\lambda = 0$ is associated with the stationary sheet case. We implement the following non-dimensional variables to render Eqns. (6)-(11) into dimensionless form:

$$x = \frac{\bar{x}}{L}, \ y = \frac{\bar{y}}{L} Ra^{1/5}, \ u = \frac{L}{\alpha} Ra^{-2/5} \bar{u}, \ v = \frac{L}{\alpha} Ra^{-1/5} \bar{u}, \ \theta = \frac{T - T_\infty}{T_w - T_\infty},$$
$$\phi = \frac{C - C_\infty}{C_\infty}, p = \frac{L^2 (\bar{p} - \bar{p}_\infty)}{\rho_f \alpha^2} Ra^{-4/5},$$

$$(12)$$

where $Ra = g \beta (1 - C_\infty)(T_w - T_\infty) L^3 \rho_f / (\alpha \mu)$ is the Rayleigh number. A non-dimensional stream function, ψ, is also introduced, defined by:

$$u = \frac{\partial \psi}{\partial y} \ \text{and} \ v = -\frac{\partial \psi}{\partial x}, \tag{13}$$

Introducing this into Eqns. (6)-(11)., Eqn. (6) is satisfied identically and the following dimensionless partial differential equations for the flow problem are arrived at:

$$\text{Pr} \frac{\partial^3 \psi}{\partial y^3} - \frac{\partial p}{\partial x} + \frac{\partial \psi}{\partial x} \frac{\partial^2 \psi}{\partial y^2} - \frac{\partial \psi}{\partial y} \frac{\partial^2 \psi}{\partial y \partial x} = 0, \tag{14}$$

$$-\frac{1}{\text{Pr}} \frac{\partial p}{\partial y} + \theta - Nr\phi = 0, \tag{15}$$

$$\frac{\partial \psi}{\partial y} \frac{\partial \theta}{\partial x} - \frac{\partial \psi}{\partial x} \frac{\partial \theta}{\partial y} - \frac{\partial^2 \theta}{\partial y^2} - Nb \frac{\partial \theta}{\partial y} \frac{\partial \phi}{\partial y} - Nt \left(\frac{\partial \theta}{\partial y} \right)^2 = 0, \tag{16}$$

$$Le \left[\frac{\partial \psi}{\partial y} \frac{\partial \phi}{\partial x} - \frac{\partial \psi}{\partial x} \frac{\partial \phi}{\partial y} \right] - \frac{\partial^2 \phi}{\partial y^2} - \frac{Nt}{Nb} \frac{\partial^2 \theta}{\partial y^2} = 0. \tag{17}$$

The boundary conditions in Eqn. (11) become

$$\frac{\partial \psi}{\partial x} = 0, \ \frac{\partial \psi}{\partial y} = -\lambda a x^{1/5} \frac{\partial^2 \psi}{\partial y^2}, \theta = 1 + b x^{-2/5} \frac{\partial \theta}{\partial y}, \ Nb\phi'(0) + Nt\theta'(0) = 0 \ \text{at} \ y = 0,$$

$$\frac{\partial \psi}{\partial y} \to 0, \ \theta \to 0, \ \phi \to 0, p \to 0 \ \text{as} \ y \to \infty. \tag{18}$$

The parameters in Eqns. (14)-(16) are Pr, Nt, Nb, Nr , Le, a and b and these designate, respectively, the thermophoresis parameter, the Brownian motion parameter, the buoyancy

ratio parameter and the Lewis number respectively, which are defined by (see **Nield and Kuznetsov 2014**):

$$\Pr = \frac{\nu}{\alpha}, Nt = \frac{\tau D_T (T_w - T_\infty)}{\alpha T_\infty}, Nb = \frac{\tau D_B C_\infty}{\alpha}, Nr = \frac{(\rho_p - \rho_f) C_\infty}{\rho_f \beta (1 - C_\infty)(T_w - T_\infty)},$$

$$Le = \frac{\alpha}{D_B}, a = \frac{(N_1)_0 \mu Ra^{2/5}}{\rho_f L}, b = \frac{(D_1)_0 Ra^{2/5}}{L}$$

(19)

2.2. Methods of solution

By applying the Lie group method to (14)-(16), the infinitesimal generator for the problem can be written as (**Cantwell 2003**):

$$X = \xi_1 \frac{\partial}{\partial x} + \xi_2 \frac{\partial}{\partial y} + \eta_1 \frac{\partial}{\partial \psi} + \eta_2 \frac{\partial}{\partial \theta} + \eta_3 \frac{\partial}{\partial \phi} + + \eta_4 \frac{\partial}{\partial p},$$

(20)

where the transformations are $(x, y, \psi, \theta, \phi, p)$ to $(x^*, y^*, \psi^*, \theta^*, \phi^*, p^*)$. The infinitesimals $\xi_1, \xi_2, \eta_1, \eta_2, \eta_3$ and η_4 satisfies the following first order differential equations:

$$\frac{dx^*}{d\varepsilon} = \xi_1(x^*, y^*, \psi^*, \theta^*, \phi^*, p^*), \frac{dy^*}{d\varepsilon} = \xi_2(x^*, y^*, \psi^*, \theta^*, \phi^*, p^*),$$

$$\frac{d\psi^*}{d\varepsilon} = \eta_1(x^*, y^*, \psi^*, \theta^*, \phi^*, p^*), \frac{d\theta^*}{d\varepsilon} = \eta_2(x^*, y^*, \psi^*, \theta^*, \phi^*, p^*),$$

(21)

$$\frac{d\phi^*}{d\varepsilon} = \eta_3(x^*, y^*, \psi^*, \theta^*, \phi^*, p^*), \frac{dp^*}{d\varepsilon} = \eta_4(x^*, y^*, \psi^*, \theta^*, \phi^*, p^*),$$

After algebraic manipulation, it is found that the forms of the infinitesimals are:

$$\xi_1 = c_1 x + c_2, \quad \xi_2 = \frac{2}{5} c_1 y + c_3,$$

$$\eta_1 = \frac{3}{5} c_1 \psi + c_4, \quad \eta_2 = c_5, \quad \eta_3 = c_6, \eta_4 = (c_5 + c_6) y + \frac{2}{5} c_1 p.$$

(22)

where $c_i (i = 1, 2, L, 6)$ are arbitrary constants. Hence, the equations admit six finite parameter Lie group transformations. It is observed that the parameter c_2, c_3 correspond to the translation in the variables x, y, while the parameter c_4 corresponds to the translation in the variable ψ. It is also noted that the parameter c_1 corresponds to the scaling in the variables x, y, ψ and p respectively. The *characteristic equation* is:

$$\frac{dx}{c_1 x + c_2} = \frac{dy}{\frac{2}{5} c_1 y + c_3} = \frac{d\psi}{\frac{3}{5} c_1 \psi + c_4} = \frac{d\theta}{c_5} = \frac{d\phi}{c_6} = \frac{dp}{-\alpha_2 (c_5 + c_6) y + \frac{2}{5} c_1 p}.$$

(23)

The similarity transformations corresponding to the characteristic Eqn. (23) are as follows

$$\eta = \frac{y}{x^{\frac{2}{5}}}, \ \psi = x^{\frac{3}{5}} f(\eta), \ p = x^{\frac{2}{5}} h(\eta), \ \theta = \theta(\eta), \ \phi = \phi(\eta) \tag{24}$$

For simplicity we assumed that $c_i = 0, (i = 3-6)$.

2.2.1 Similarity equations

On substituting the transformations of Eqn. (24) into the governing Eqns. (14)- (17), we obtain the following similarity equations:

$$\Pr f''' + \frac{3}{5} ff'' - \frac{1}{5} f'^2 + \frac{2}{5} \eta h' - \frac{2}{5} h = 0, \tag{25}$$

$$-\frac{1}{\Pr} h' + \theta - Nr \ \phi = 0, \tag{26}$$

$$\theta'' + \frac{3}{5} f \ \theta' + Nb \ \theta' \ \phi' + Nt \ \theta'^2 = 0, \tag{27}$$

$$\phi'' + \frac{3}{5} Le f \ \phi' + \frac{Nt}{Nb} \theta'' = 0. \tag{28}$$

The relevant boundary conditions are:

$$\begin{array}{l} f(0) = 0, \ f'(0) = \lambda + a \ f''(0), \ \theta(0) = 1 + b \ \theta'(0), \ Nb \ \phi'(0) + Nt \ \theta'(0) = 0, \\ f'(\infty) = \theta(\infty) = \phi(\infty) = h(\infty) = 0, \end{array} \tag{29}$$

where primes denote differentiation with respect to η.

It is worth mentioning that in the case of stationary sheet (plate) with no-slip boundary conditions at wall ($a = b = \lambda = 0$), the problem under consideration reduces to that which has been recently investigated by **Pradhan et al. (2014)**.

2.3 Physical Quantities (Local Skin Friction & Nusselt number)

These quantities can be calculated from the following relations:

$$C_{f\bar{x}} = \frac{2\mu}{\rho U_r^2} \left(\frac{\partial \bar{u}}{\partial \bar{y}} \right)_{\bar{y}=0}, \ Nu_{\bar{x}} = \frac{-\bar{x}}{T_w - T_\infty} \left(\frac{\partial T}{\partial \bar{y}} \right)_{\bar{y}=0}. \tag{30}$$

By substituting from Eqns. (12) and (31) into Eqn. (37), we get :

$$Ra_{\bar{x}}^{7/5} \Pr C_{f\bar{x}} = f''(0), \ Ra_{\bar{x}}^{-1/5} Nu_{\bar{x}} = -\theta'(0). \tag{31}$$

Here $Ra_{\bar{x}} = g\,\beta(1-C_\infty)\Delta T\,\bar{x}^3/(\alpha\nu)$ is the local Rayleigh number. Here $U_r = g\,\beta(1-C_\infty)(T_w - T_\infty)L^2/\alpha$ is the characteristic velocity. Due to zero mass flux boundary conditions, there will be no mass flux at the boundary.

2.4. Numerical Solution

The inspiration behind this scheme is that one can now solve the normalized boundary value problem, although nonlinear, quite easily, both using analytic and numerical schemes. The most widely employed numerical method for the boundary value problems is the collocation method. The advantage of this method is that, it reduces the nth order differential equation(s) into n first order differential equations, thus reducing the computational cost on a large domain with small step size and a range of parameters. We have simplified the system of equations (25)-(28) using the Generalized Collocation Method (GCM). Collocation methods are basically implicit Runge-Kutta quadrature techniques. They are well documented in numerous monographs including **Ascher et al. (1998)** and **Isaacson and Keller (1966)**. The reader is referred to these sources for further details. As with all numerical procedures employed for solving boundary value problems with infinity boundary conditions, a sufficiently large value of the coordinate at infinity is required to ensure asymptotically smooth profiles and convergence to the correct solution. In the present computations this has been carefully addressed as testified to by all the figures plotted. Generally it is found that the order of a collocation method is related to the order of the quadrature rule which is developed by utilizing the collocation points as weighting coefficients in the stepping algorithm. Collocation methods in nonlinear multi-physical boundary layer flows including magnetohydrodynamics are also described in detail in **Bég (2012).** For the validation of our numerical solution, we have solved the system of Eqns. (25)-(28) subject to the boundary condition (30). We have presented the comparison in **Table 1** and **Table 2** to show that for *λ=0*, our results are in agreement with the results of **Pradhan *et al.* (2014)**. After the validation, we have conducted general numerical simulations subject to a set of parametric values.

3. RESULTS

Comprehensive computations have been presented in **Figs. 2-11** for the influence of the evolving thermophysical parameters on the dimensionless velocity, temperature, nanoparticle concentration, heat transfer rates and the skin friction. We confine our attention to the influence of the velocity slip (*a*), thermal slip (*b*), stretch/shrink parameter (*λ*), thermophoresis *(Nt)* and Lewis number *(Le)*. In all cases *Pr =6.8, Nt =Nb =0.2 i.e., this corresponds to water-based nanofluid with weak thermophoresis and intermediate nano-particle sizes.*

4. DISCUSSION

Figures 2-4 depict the effect of sheet stretching/shrinking parameter (*λ*) and velocity slip parameter (*a*) on the dimensionless velocity and temperature. Evidently near the sheet, increasing velocity slip accelerates the flow velocity inside the boundary layer for a shrinking sheet ($\lambda = -0.1$) and static sheet ($\lambda = 0$) as well as a stretching sheet ($\lambda = 0.1$). It is further found that velocity increases for both slip flow and non-slip flow, as the Lewis number parameter increases. For the conventional no-slip case with sheet-shrinking (*a=0, λ=-0.1*), negative velocities are in fact produced at the sheet and in close proximity to it. The sheet-shrinking is therefore, in this case, responsible for inducing a significant backflow in the vicinity of the sheet surface. It is also observed that higher temperatures are achieved for the no-slip scenario (*a=0*); and the lowest temperatures correspond to the strong slip case (*a=0.2*) for a shrinking sheet ($\lambda = -0.1$) and static sheet ($\lambda = 0$) as well as a stretching sheet ($\lambda = 0.1$). Thermal boundary layer thickness will therefore be reduced with greater slip effects. Lewis number is found to decrease the temperature for a shrinking sheet ($\lambda = -0.1$) and static sheet ($\lambda = 0$) as well as a stretching sheet ($\lambda = 0.1$).

Figures 5-7 depict the effect of the thermal slip and sheet stretching/shrinking parameter (*λ*) on the dimensionless velocity and temperature. It emerges that increasing thermal slip *decelerates* the flow inside the boundary layer for a shrinking sheet ($\lambda = -0.1$) and static sheet ($\lambda = 0$) as well as a stretching sheet ($\lambda = 0.1$). Velocity apparently also increases both in the presence and absence of thermal slip as the Lewis number rises. Lewis number is directly proportional to the nanofluid thermal diffusivity and inversely proportional to the nanoparticle diffusivity. In all the computations presented, *Le ≥0*. Both heat and nanoparticle species diffuse at the same rate for *Le* = 1 whereas for *Le* > 1 the heat diffusion rate exceeds the species diffusion rate. Increasing Lewis number therefore accelerates the nanofluid boundary layer

flow. There is an intimate connection between the diffusion rate of vorticity (viscosity effect) and heat and species diffusion. Boundary layer structures (thicknesses) are modified by these rates. Further, from Figs. 4-6, it is observed that higher temperatures are achieved for the no-slip scenario (*b=0*); and the lowest temperature corresponds to the strong thermal slip case (*b=0.2)* for a shrinking sheet ($\lambda = -0.1$) and static sheet ($\lambda = 0$) as well as a stretching sheet ($\lambda = 0.1$). Thermal boundary layer thickness will therefore be increased with greater thermal slip effects. This has important implications in materials processing since heat control rates at the wall can be manipulated with wall slip (thermal jump).

Figure 8 depicts the effects of the thermal slip and sheet stretching/shrinking parameter (λ) on the dimensionless nanoparticle volume fraction. An elevation in thermal slip increases the nanoparticle concentration for the static sheet ($\lambda = 0$) as well as a stretching sheet ($\lambda = 0.1$). However nanoparticle volume fraction decreases for both in the presence of thermal slip and absence of thermal slip as the Lewis number parameter rises.

Figures 9-11 depict the effect of the various parameters on the dimensionless friction and the heat transfer rates. It is observed that the friction is decreased as the thermophoresis parameter and buoyancy ratio parameter are decreased for both slip flow and conventional no-slip flow. Friction is decreased as the velocity slip parameter increased. It is further seen from these figures that heat transfer rate reduces with the thermophoresis and buoyancy ratio parameters for stretching sheet, stationary sheet and indeed also for a shrinking sheet for both the slip and no-slip cases. Velocity slip leads to a rise in wall temperature gradient.

5. CONCLUSIONS

Steady-state nanofluid flow from a horizontal plate has been investigated by a combined Lie group and numerical analysis techniques. Velocity and thermal slip effects, which are of interest in materials processing operations**,** have also been incorporated. Passively controlled boundary condition have been used to attain more robust results. With the aid of a Lie algebraic group method, the boundary layer equations for momentum, energy and species diffusion (nanoparticle concentration) have been reduced to a nonlinear, coupled system of ordinary differential equations. The resulting two-point boundary value problem has been solved numerically using generalized collocation method. Solutions have been verified with established published results and very good correlation obtained. The heat, mass and

momentum characteristics have been shown to be controlled by a number of thermophysical parameters including Brownian motion, thermophoresis, Lewis number, Prandtl number, velocity slip, thermal slip, buoyancy ratio and sheet stretch/shrink parameter. The present computations have shown that:

(i) Increasing velocity slip is found to depress temperature and friction whereas it enhances velocity and heat transfer rates.

(ii) Increasing thermal slip reduces velocity whereas it elevates temperature and nanoparticle concentration.

(iii) Wall friction is decreased as the thermophoresis parameter and buoyancy ratio parameter are decreased for both slip flow and conventional no slip flow.

(iv) Heat transfer rates are reduced with the thermophoresis parameter and buoyancy ratio parameters for stretching, stationary and shrinking sheet cases, for both the slip and no-slip cases. Velocity slip also leads to a rise in wall temperature gradient.

The present study has been confined to steady flat sheet flow; future studies will consider transient inclined sheet nanofluid flows, and will be communicated soon.

REFERENCES

Adnan H, Sharma KV, Bakar RA, Kadirgama K, A review of forced convection heat transfer enhancement and hydrodynamic characteristics of a nanofluid, *Renew and Sus Ener Rev* **29**: 734, 2014.

Ali H M, Ali H, Liaquat H, Maqsood HT, Nadir MA, Experimental investigation of convective heat transfer augmentation for car radiator using ZnO water nanofluids, Energy **84**:1, 2015

Ascher, Uri M.; Petzold, Linda R, *Computer Methods for Ordinary Differential Equations and Differential-Algebraic Equations*, Society for Industrial and Applied Mathematics, Philadelphia, USA (1998).

Buongiorno J, Convective transport in nanofluids, *ASME J Heat Trans* **128**: 240, 2006.

Choi S, Enhancing thermal conductivity of fluids with nanoparticles, *Developments and applications of non-Newtonian flows, D. A. Siginer and H. P., Wang, eds., American Society of Mechanical Engineers*, New York, FED- Vol. 231/MD **66**: 99,1995.

Coumaressin T, Palaniradja K, Performance analysis of a refrigeration system using nanofluid, *Int J Adv Mec Eng* **4**:459,2014.

Das S K, Choi SUS, Yu W, Pradeep T, *Nanofluids: Science and Technology*, 1st ed., Wiley, New York, 2007.

Das SK, Choi SU, A review of heat transfer in nanofluids, *Adv Heat Transf* **46**, 119, 2009.

Dehghan M, Mahmoudi Y, Valipour MS, Saedodin S, Combined conduction–convection–radiation heat transfer of slip flow inside a micro-channel filled with a porous material, *Transp in Porous Med* **108**:413, 2015.

Cantwell, B.J., *Introduction to Symmetry Analysis*, Cambridge University Press (2003).

Ferdows M, Khan MS, Bég OA, Azad MAK, Alam MM, Numerical study of transient magnetohydrodynamic radiative free convection nanofluid flow from a stretching permeable surface, *Proc. IMechE-Part E: J Process Mech Eng* **228**:181,2014.

Isaacson E, Keller HB, *Analysis of Numerical Methods*, John Wiley, USA (1966).

Kakac S, Pramuanjaroenkij A, Review of convective heat transfer enhancement with nanofluids, *Int J Heat MassTransf* **52**: 3187, 2009.

Karniadakis G, Beskok A, Aluru N, Microflows and Nanoflows Fundamentals and Simulation. In: *Microflows and Nanoflows Fundamentals and Simulation*. Springer Science, New York, USA (2005).

Kuznetsov AV, Nield DA, Natural convective boundary- layer flow of a nanofluid past a vertical plate, *Int J Therm Sci* **49**:243, 2010.

Kuznetsov AV, Nield DA, Natural convective boundary-layer flow of a nanofluid past a vertical plate: A revised model, *Int J Ther Sci* **77**:126, 2014.

Mahdi RA, Mohammed HA, Munisamy KM, Saeid NH, Review of convection heat transfer and fluid flow in porous media with nanofluid, *Renew and Sus Ener Rev* **41**:715,2015.

Mauro L, Colangelo G, Milanese M, de Risi A, Review of heat transfer in nanofluids: Conductive, convective and radiative experimental results, *Renew and Sus Ener Rev* **43**: 1182, 2015.

Maxwell-Garnett JC, Colours in metal glasses and in metallic films, *Philos Trans R Soc London, Ser A*, 203:385, 1904.

Minkowycz WJ, Sparrow EM, Abraham JP, *Nanoparticle Heat Transfer and Fluid Flow*, CRC Press, Boca Raton, Florida, USA (2012).

Murshed SMS, Leong KC, Yang C, *Thermophysical Properties of Nanofluids,* CRC Press, New York (2011).

Nield DA, Kuznetsov AV, The Cheng-Minkowycz problem for natural convective boundary-layer flow in a porous medium saturated by a nanofluid, *Int J Heat Mass Transfer* **52**: 5792, 2009.

Nield DA, Kuznetsov AV, The Cheng-Minkowycz problem for the double-diffusive natural convective boundary-layer flow in a porous medium saturated by a nanofluid, *Int J Heat Mass Transf* **54:**374, 2011.

Pak BC, Cho Y, Hydrodynamic and heat transfer study of dispersed fluids with submicron metallic oxide particles, *Exp Heat Transf* **11**:151, 1998.

Pradhan K, Samanta S, Guha A, Natural convective boundary layer flow of nanofluids above an isothermal horizontal plate, *ASME J. Heat Transf* **136**:102501, 2014.

Sattler KD, *Handbook of Nanophysics: Nanomedicine and Nanorobotics*, CRC Press, New York, USA (2010).

Sheikholeslami M, Gorji-Bandpya M, Vajravelu K, Lattice Boltzmann simulation of magnetohydrodynamic natural convection heat transfer of Al2O3–water nanofluid in a horizontal cylindrical enclosure with an inner triangular cylinder, *Int J Heat Mass Transf* **80**:16,2015.

Sonawane S, Bhandarkar U, Puranik B, Kumar SS, Convective heat transfer characterization of aviation turbine fuel-metal oxide nanofluids, *AIAA J Thermophy and Heat Transf* **26**:619, 2012.

Suleimanov BA, Ismailov FS, Veliyev EF, Nanofluid for enhanced oil recovery, *J Pet Sci and Eng* **78**: 431, 2011.

Tominaka S, Nishizeko H, Mizuno J, Osaka T, Bendable fuel cells: on-chip fuel cell on a flexible polymer substrate, *Energy Environ Sci* **2:**1074,2009.

Vleggaar I, Laminar boundary layer behaviour on continuous, accelerating surfaces, *Chem Eng Sci* **32**, 1517, 1977.

Wang BX, Zhou LP, Peng XF, A Fractal model for predicting the effective thermal conductivity of liquid with suspension of nanoparticles, *Int J Heat Mass Transfer* **46**:2665, 2003.

Wang XQ, Mujumdar AS, Heat transfer characteristics of nanofluids: a review, *Int J Therm Sci* **46:**1, 2007.

Xuan Y, Li Q, Investigation on convective heat transfer and flow features of nanofluids, *ASME J Heat Transf* **125**:151,2003.
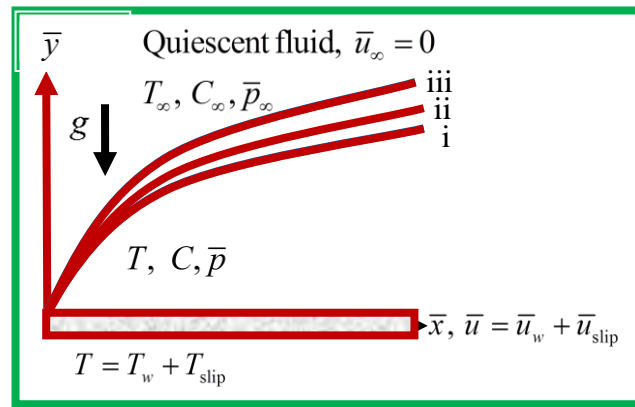
FIGURES:

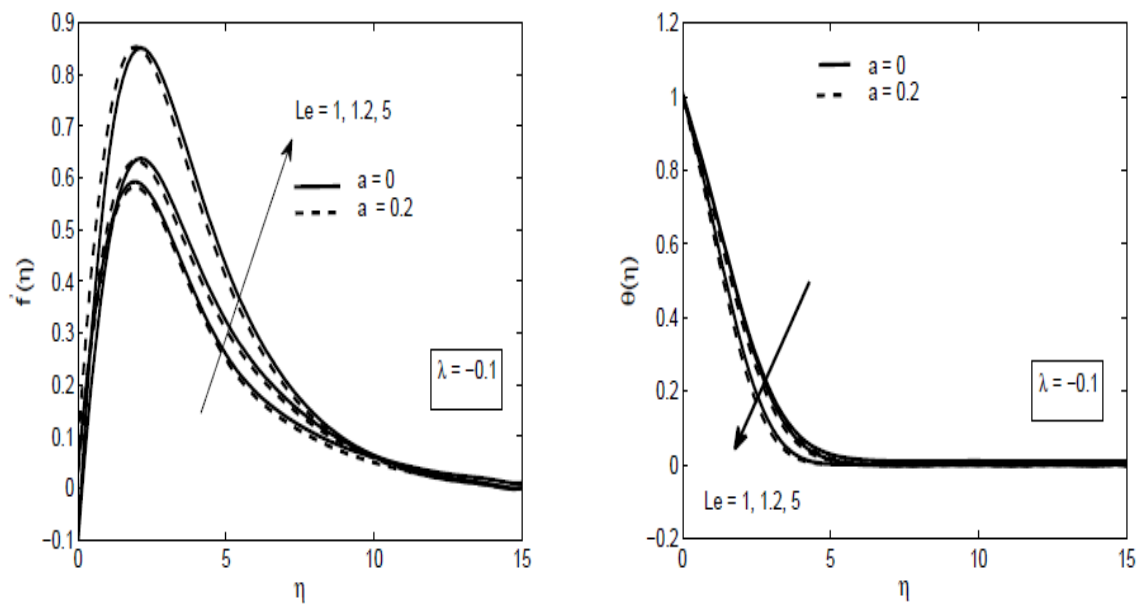**Figure 1**: Flow model and coordinate system.

Figure 2: Variation of the velocity distribution $f'(\eta)$ and temperature $\theta(\eta)$ of the nanofluid for three values of Le at *Pr=6.8, Nr=0.5, Nt=Nb=0.2, b = 0.1 and λ= -0.1.*
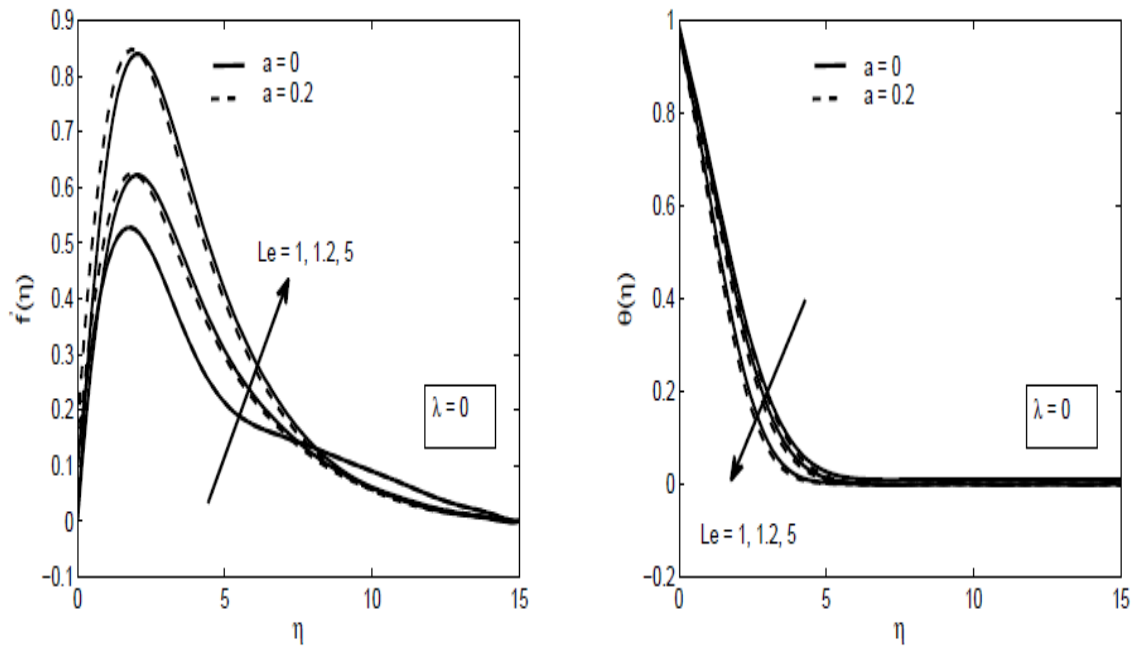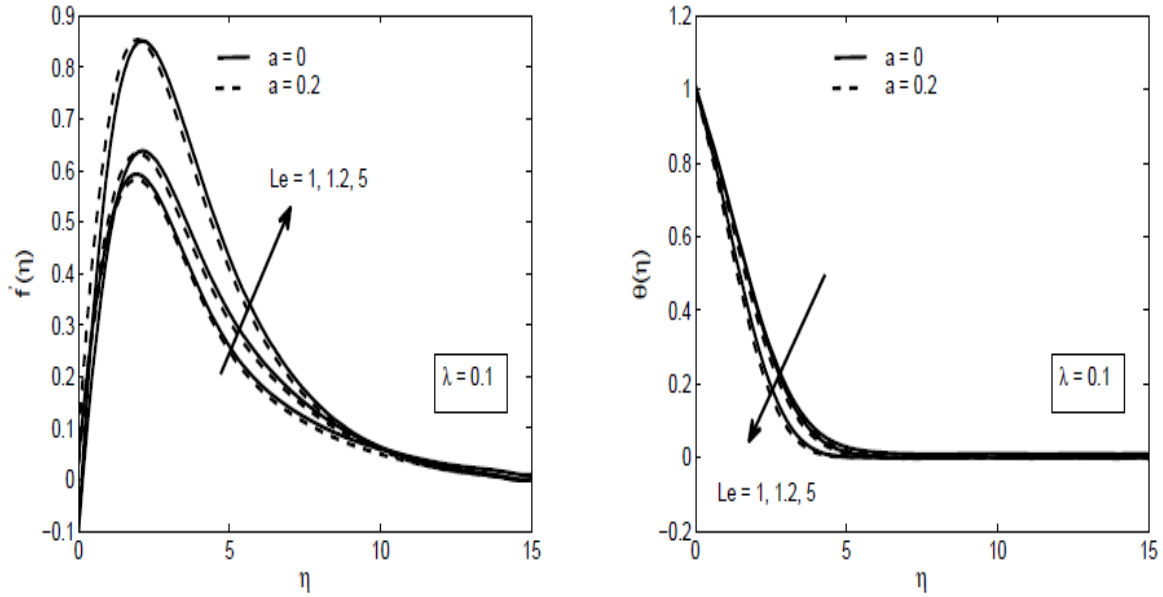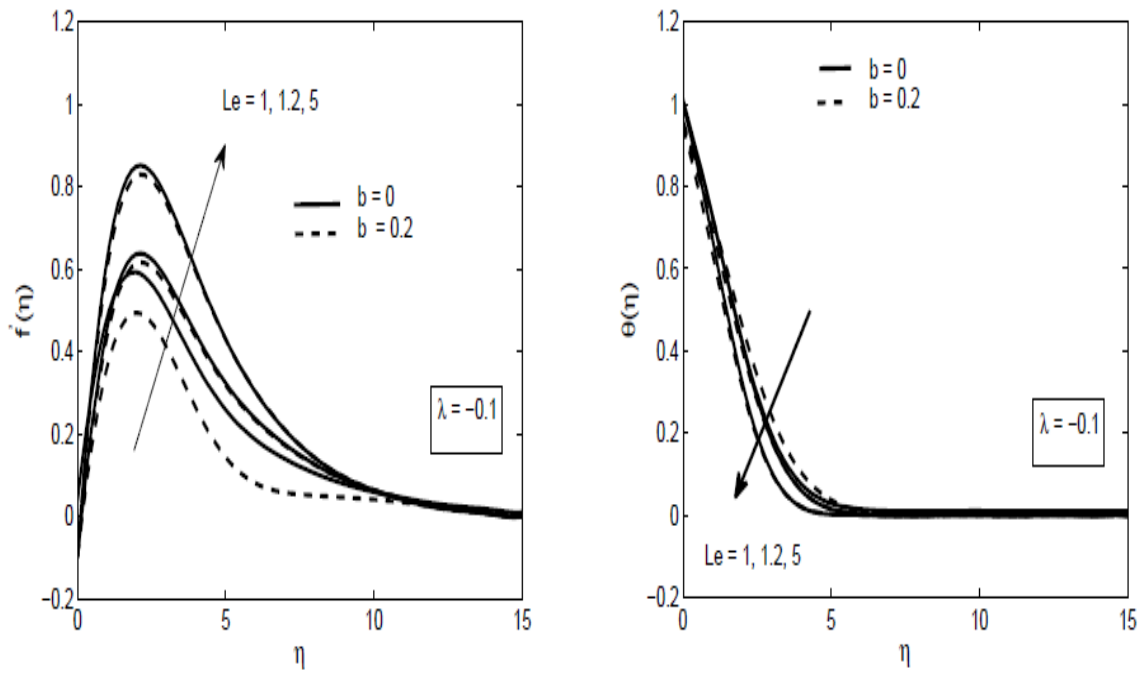
Figure 3: Variation of the velocity distribution $f'(\eta)$ and temperature $\theta(\eta)$ of the nanofluid for three values of Le at *Pr = 6.8, Nr = 0.5; Nt = Nb = 0.2, b = 0.1 and λ=0.*
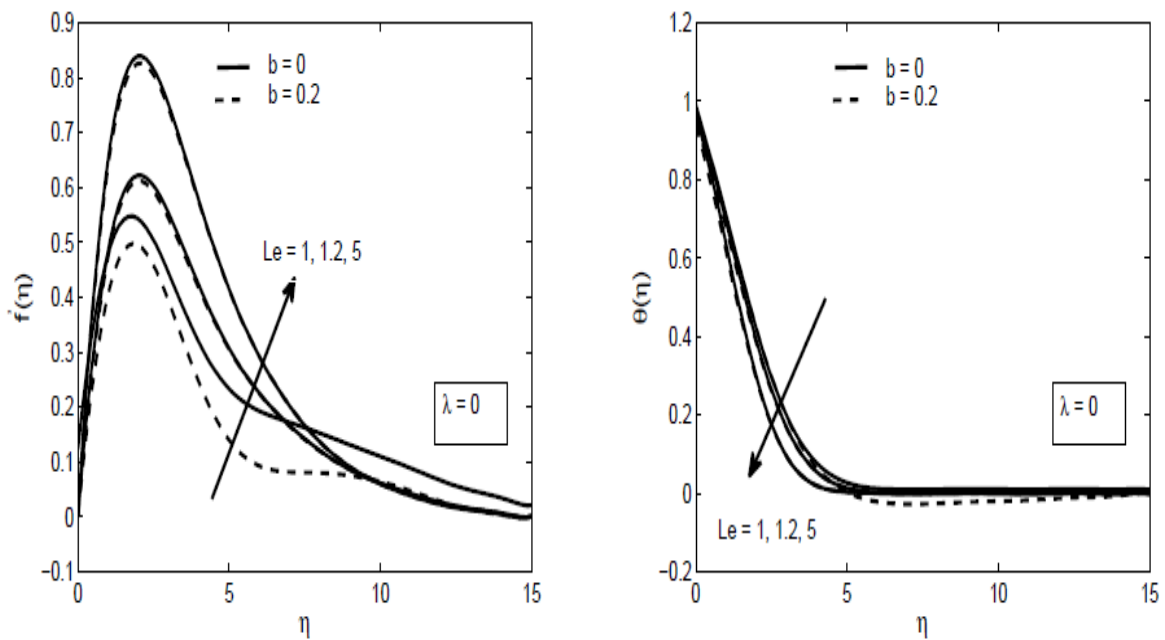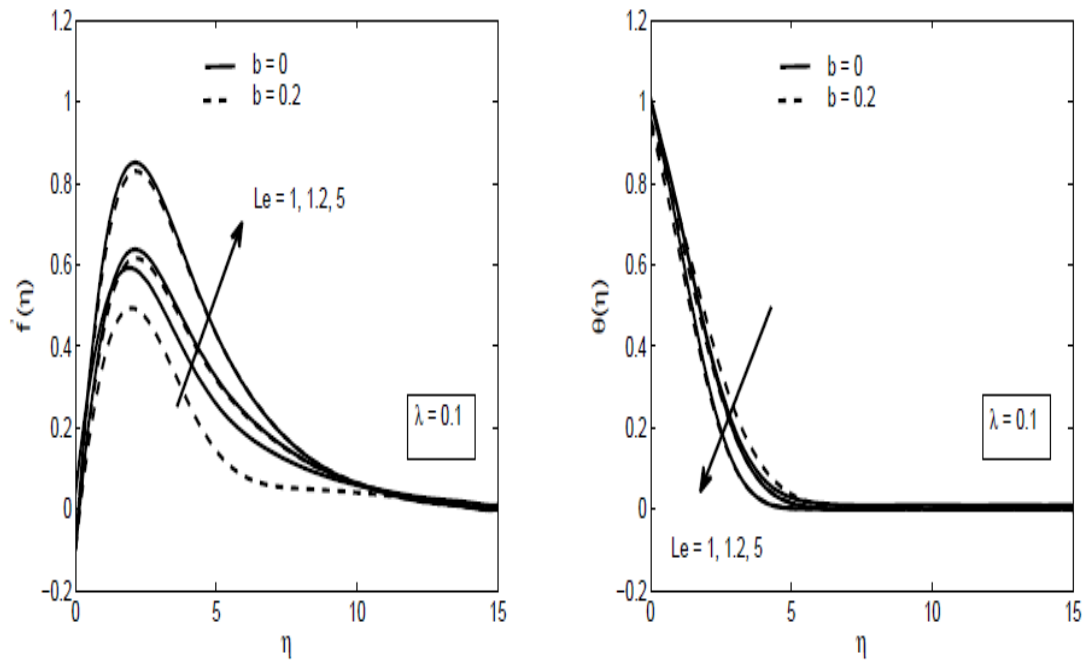

Figure 4: Variation of the velocity distribution $f'(\eta)$ and temperature $\theta(\eta)$ of the nanofluid for three values of Le at *Pr = 6.8, Nr = 0.5; Nt = 0.2; Nb = 0.2, b = 0.1 and λ= 0.1.*

Figure 5: Variation of the velocity distribution $f'(\eta)$ and temperature $\theta(\eta)$ of the nanofluid for three values of Le at *Pr = 6.8, Nr = 0.5; Nt = Nb = 0.2, a = 0.1 and λ = -0.1*.

Figure 6: Variation of the temperature distribution $\theta(\eta)$ and velocity $f'(\eta)$ of the nanofluid for three values of Le at *Pr = 6.8, Nr = 0.5; Nt =Nb = 0.2, a = 0.1 and λ= 0*.

Figure 7: Variation of the velocity distribution $f'(\eta)$ and temperature $\theta(\eta)$ of the nanofluid for three values of Le at $Pr = 6.8$, $Nr = 0.5$; $Nt = Nb = 0.2$, $a = 0.1$ and $\lambda = 0.1$.
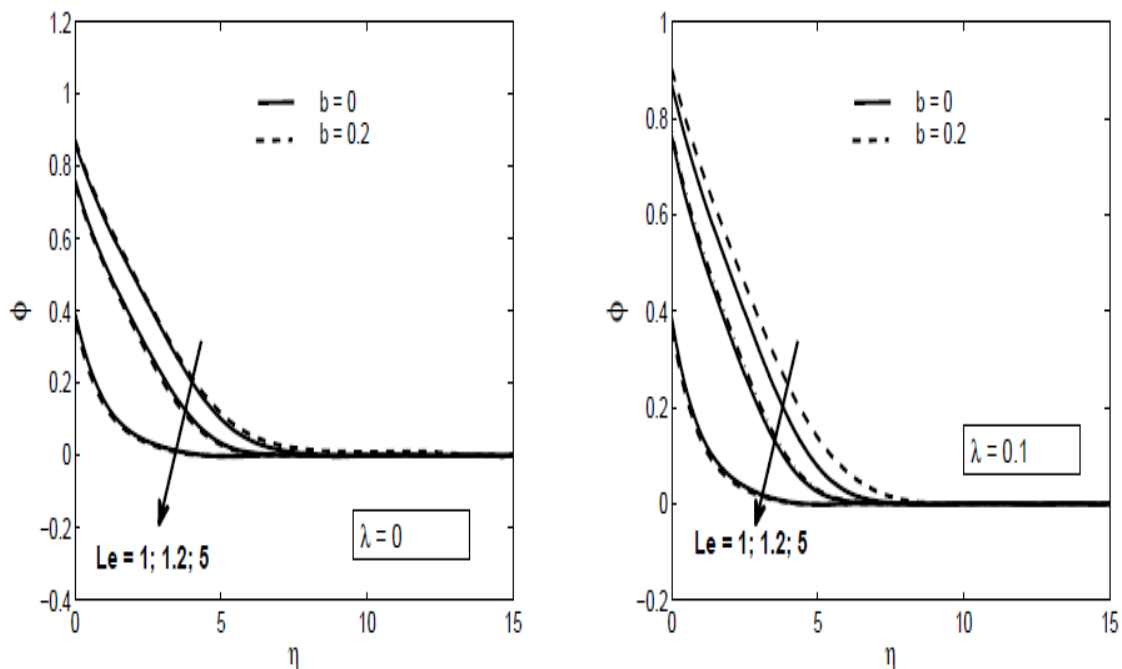

Figure 8: Variation of the nanoparticle volume fraction distribution $\phi(\eta)$ for three values of Le at $Pr = 6.8$, $Nr = 0.5$; $Nt = Nb = 0.2$, $a = 0.1$ and $\lambda = 0.1$.
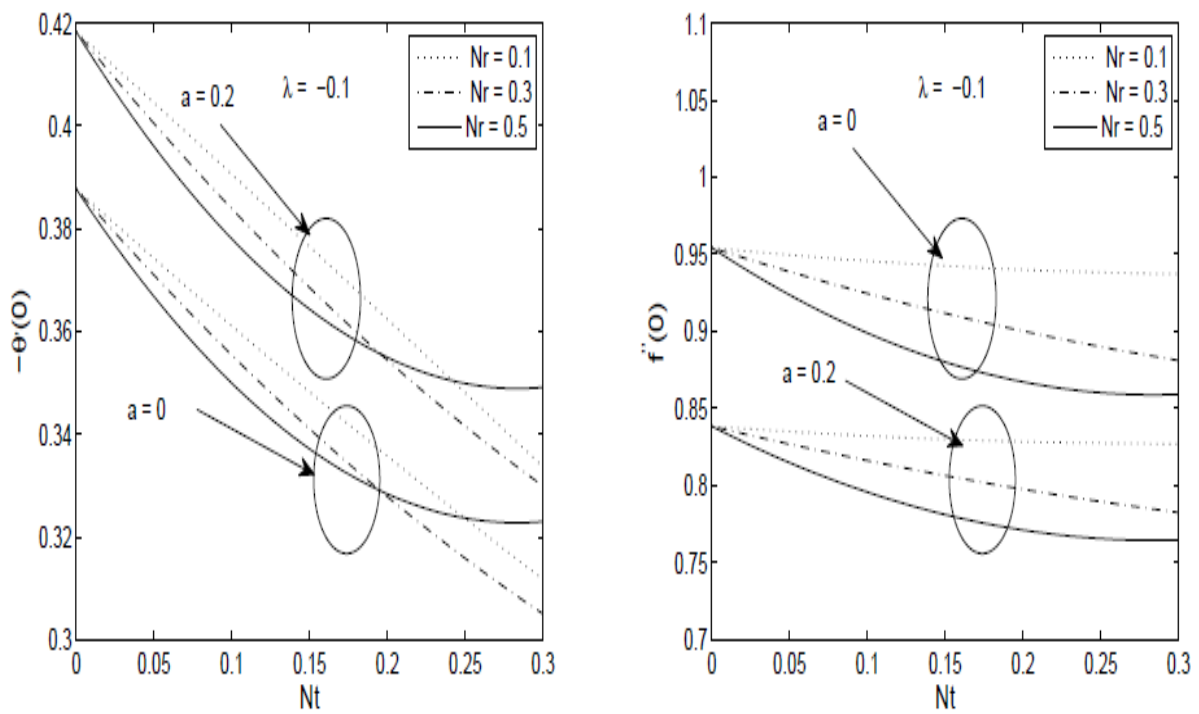
Figure 9. The reduced local Nusselt number and the reduced local skin-friction coefficient relative to thermophoretic parameter for *Pr =6.8, Le =5, Nb =0.2 and λ=-0.1*.
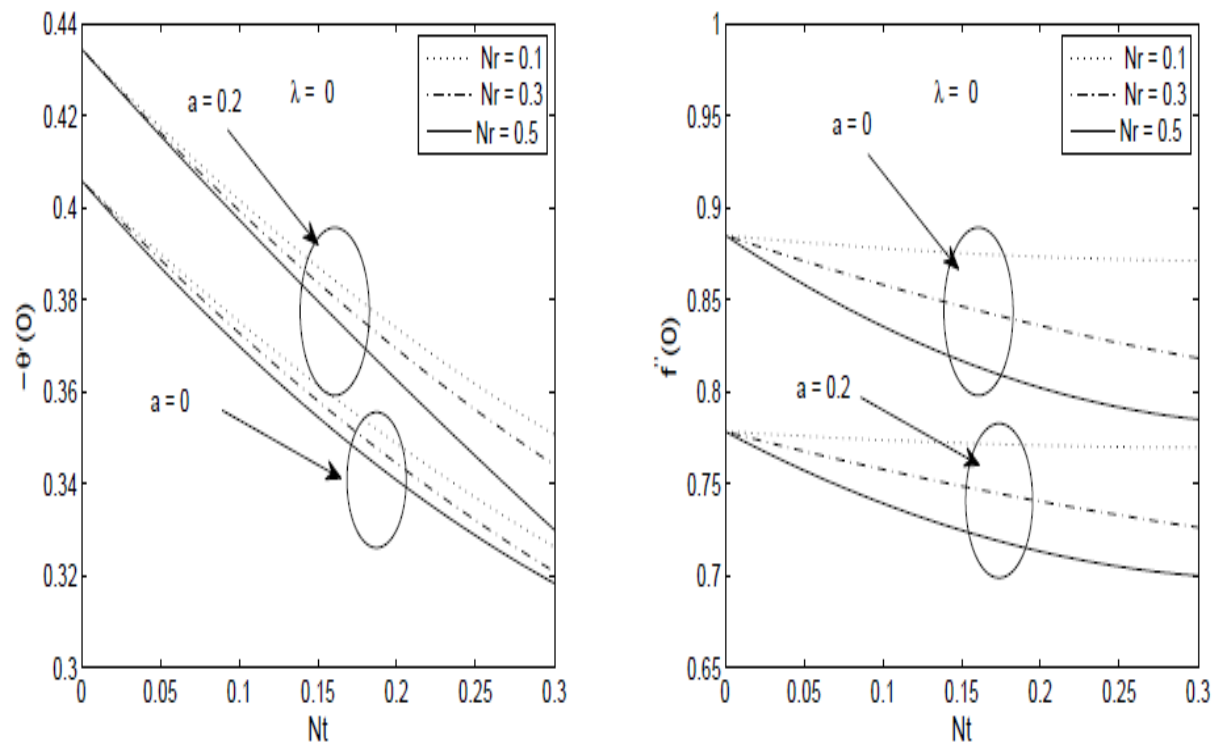

Figure 10: The reduced local Nusselt number and the reduced local skin-friction coefficient relative to thermophoretic parameter for Pr = 6.8, Le = 5, Nb = 0.2 and λ = 0.
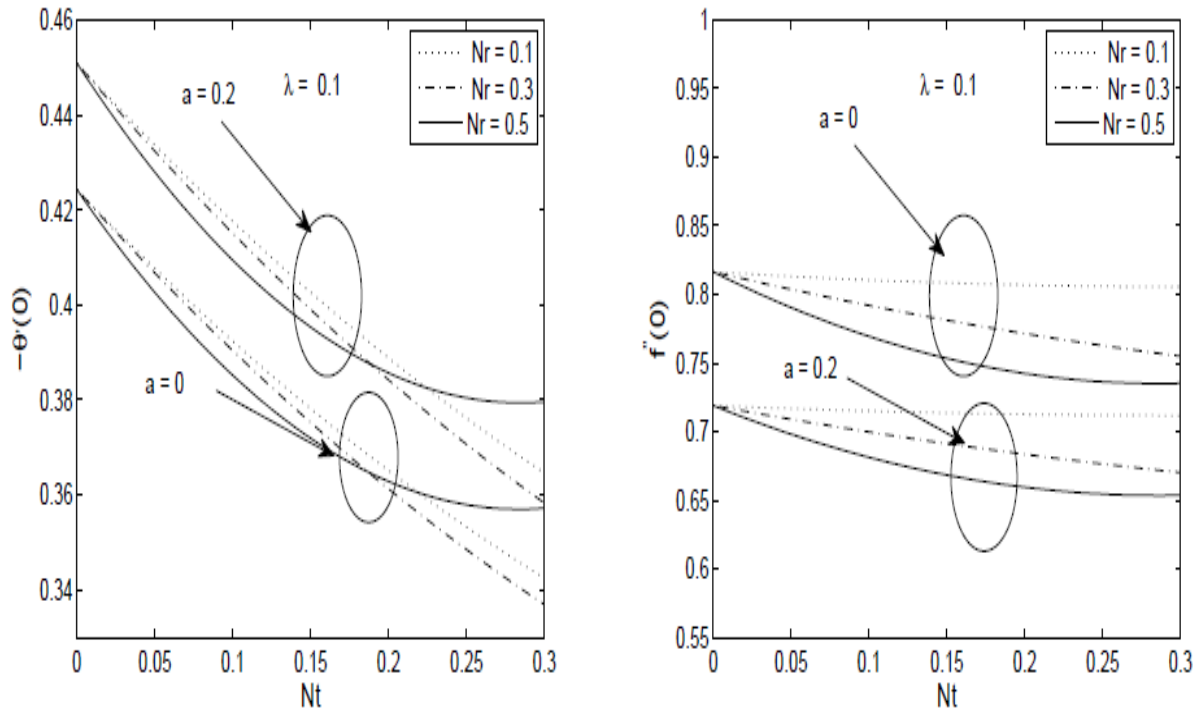
Figure 11: The reduced local Nusselt number and the reduced local skin-friction coefficient relative to thermophoretic parameter for *Pr = 6.8, Le = 5, Nb = 0.2 and λ = -0.1*.

Table 1: Values of the reduced skin friction coefficient $f''(0)$ for *Nr=Nt=Nb=0.5, Pr =6.8*.

	Pradhan _et al._ (2014)	Present work		
Le		$(\lambda = -0.1)$	$(\lambda = 0))$	$(\lambda = 0.1)$
5	0.8435	0.8276	0.8435	0.7001
10	0.8806	0.8612	0.8806	0.7506
100	0.9217	0.9106	0.9218	0.7815

Table 2: Values of the reduced Nusselt number $-\theta'(0)$ for *Nr=Nt=Nb =0.5, Pr = 6.8*.

	Pradhan _et al._ (2014)	Present work		
		$(\lambda = -0.1)$	$(\lambda = 0)$	$(\lambda = 0.1)$
Le				
5	0.3268	0.3142	0.3265	0.3310
10	0.3239	0.3095	0.3238	0.3295
100	0.3135	0.3081	0.3134	0.3086